Journal of Sol-Gel Science and Technology (2019) 91:496–504
https://doi.org/10.1007/s10971-019-05064-6

ORIGINAL PAPER: NANO- AND MACROPOROUS MATERIALS (AEROGELS, XEROGELS, CRYOGELS, ETC.)

Check for updates

Facile preparation of HNT/PVOH aerogels and the construction of PVOH-assisted HNT three-dimensional network

Hongli Liu[1] · Shixiong Li[1] · Hongyan Li[1] · Xiang He[1] · Jing Li[1] · Yajing Li[1]

Received: 11 December 2018 / Accepted: 21 June 2019 / Published online: 3 July 2019

Abstract

Halloysite nanotube/polyvinyl alcohol (HNT/PVOH) aerogel composites have been successfully prepared via an environmentally friendly freeze-drying process, by using water as solvent and borax solution as a cross-linking agent. These aerogel composites have a three-dimensional network structure formed by PVOH adhered to HNTs. The microstructure of aerogels and the interface adhesion between HNTs and PVOH were investigated by scanning electron microscopy and transmission electron microscopy. Meanwhile, thermal conductivity, compressive strength, and thermal stability were measured by related instruments. The results showed that HNT/PVOH aerogels were successfully synthesized and that HNTs firmly connected to PVOH played the role as a skeleton for aerogels and effectively enhanced the mechanical properties. As the content of HNTs increased, the obtained aerogel materials exhibited a decrease in thermal conductivity, an increase in compressive strength, an improvement in thermal stability, and formation of a locally dense PVOH network. Moreover, microstructure models were established by electron microscopic images to analyze the results in detail. Importantly, there is no need for the formation of block hydrogel during the synthetic process and these HNT/PVOH aerogel composites could be fabricated easily and quickly from cheap raw materials, contributing to large-scale production.

Graphical Abstract

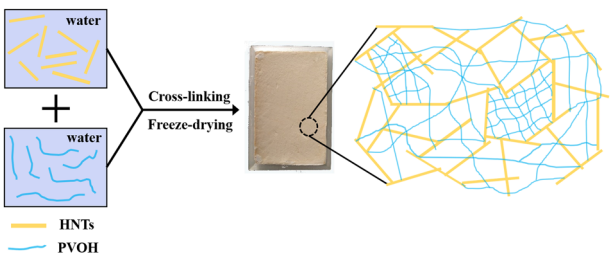

Highlights

- These composites are easy to fabricate and environmentally friendly in the preparation process.
- PVOH was adhered to HNTs to form a polymer-assisted three-dimensional network structure.
- The structure and properties were analyzed in detail by microscopic models that were depicted by SEM and TEM images.

Keywords HNTs/PVOH · Microstructure models · Thermal stability

1 Introduction

Clay aerogel is a kind of nanoporous material with low cost, low density, high thermal insulation, and good mechanical strength [1–4]. A two-stage process is usually adopted to

✉ Hongli Liu
liuhongli@tcu.edu.cn

[1] School of Materials Science and Engineering, Tianjin Chengjian University, 300384 Tianjin, China

prepare this kind of aerogel, a solid clay gel is formed at the first stage, and then a facile and environmentally friendly freeze-drying process is performed to replace the ice crystal with air [5–7]. This material with nanoscale structure has shown many promising properties in a variety of applications.

Halloysite nanotubes (HNTs) are a type of naturally occurring fibrous aluminosilicate ($Al_2(OH)_4Si_2O_5{\cdot}nH_2O$) with proven biocompatibility and can be supplied in large amounts at low prices [8, 9]. HNTs are composed of a hollow cylinder formed by a plurality of rolled kaolinite layers, which are attractive compared with other minerals in the kaolinite, due to their large specific surface areas and highly mesoscopic/macroscopic pore structure [10]. The layer unit consists of outside-in alternate corner-shared tetrahedral SiO_4 sheets and edge-shared octahedral AlO_6 sheets stacked in a 1:1 stoichiometric ratio [8]. The length of HNTs ranges from 0.2 to 2 μm, and the inner and outer diameters of the tubes range from 10 to 40 nm and 40 to 70 nm, respectively [11, 12]. It has been reported that HNTs have proven to be an ideal enhancer for the manufacture of polymer composites with improved mechanical properties [13–16]. Yang et al. [17] had studied the performance of polyhydroxyalkanoate (PHA) composites reinforced by HNTs. Their results showed that the mechanical properties of PHA can be effectively improved by adding HNTs. The strength and modulus of PHA/HNT composites significantly enhanced when the HNT content is 4 wt%. Wei et al. [18] fabricated HNT/GO (graphene oxide) composite aerogels for wastewater treatment. The addition of HNTs improved the performance of GO, such as mechanical stability, specific surface area, pore volume, and many other properties.

However, natural untreated HNTs have very low chemical reactivity and are unable to construct an effective three-dimensional network by themselves [19, 20]. To fabricate clay aerogels of HNTs, various strategies are being employed by researchers. There are a number of practices that modify the HNTs to improve their dispersion in water, which are then compounded with other inorganic aerogels [21–23]. He et al. [24] grafted isooctyl functional groups onto HNTs by using *N*,*N*-dimethylformamide (DMF) to prevent their aggregation. The uniformity and compressive strength of the resultant aerogels were significantly enhanced. Nevertheless, many of the raw materials they used, such as DMF, are not environmentally friendly, and the addition of silica results in performance degradation [25, 26]. In addition, a common and effective method is to introduce polyvinyl alcohol (PVOH), which will adhere to halloysite, and the PVOH is easily cross-linked to form a three-dimensional network aerogel. Chen et al. [27] conducted a lot of research on clay/PVOH composite aerogels, and the samples they prepared showed good flame retardancy. Most of the clays they used were lamellar, and such aerogels with a "house of cards" structure are common. Their research on clay/PVOH aerogels focused on combustion performance without much characterization of microstructures. The addition of PVOH could control the microstructure of HNT clay aerogel, resulting in a uniform three-dimensional network structure of micrometer–nanometer scale.

In this study, monolithic fibrous clay/polymer aerogel composites were fabricated by using water as solvent and borax solution as a cross-linking agent. Owing to the good strength of the fibrous clay, it is possible to avoid the use of costly supercritical-drying equipment during the drying process and switching to an environmentally friendly freeze-drying method. The microstructure was characterized by scanning electron microscopy (SEM) and transmission electron microscopy (TEM). The thermal conductivity and compressive strength were tested by using a thermal conductivity detector and electronic universal testing machine, respectively. The thermal stability was analyzed by thermal gravimetric analyzer (TGA). In addition, microstructure models of HNT/PVOH aerogels were used to analyze the performance and influences of the HNT:PVOH ratio in detail.

2 Experimental section

2.1 Reagents

PVOH (Mw≈95,000) was supplied by Guangfu Fine Chemical Research Institute (Tianjin, China). HNTs with industrial grade were provided by Fenghong Clay Chemical Co., Ltd. (Zhejiang, China). Borax ($Na_2B_4O_7{\cdot}10H_2O$) was obtained from Jiangtian Chemical Technology Co., Ltd. (Tianjin, China). The deionized water used in all experiments was obtained from Millipore water purification system. All the chemicals and reagents were used without further purification.

2.2 Preparation of HNT/PVOH aerogel composites

To produce an aerogel that contains 5 wt% HNTs and 5 wt% PVOH, for example, 5 g of PVOH was dissolved in 45 mL of deionized water and then magnetically stirred for 5 h in an 80 °C water bath, followed by ultrasonic processing for 10 min. Five grams of HNTs were blended with 45 mL of deionized water, followed by ultrasonic treatment for 10 min to obtain HNT suspension. The resulting mixture of HNT suspension and PVOH solution were poured into a 200-ml beaker. Subsequently, 2 ml of borax-saturated solution was dripped into the mixture. The viscous colloidal mixture was poured into an aluminum mold (100 × 50 ×

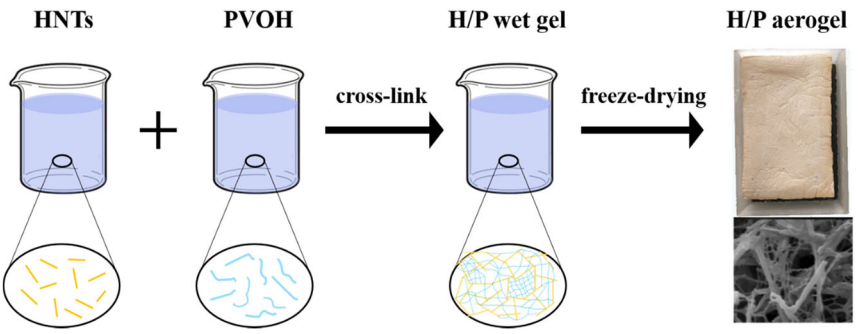

Scheme 1 The fabrication process of halloysite nanotubes/polyvinyl alcohol aerogel

20 mm^3) and then placed in a freezer at −25 °C for 24 h. The frozen samples were dried in an environmentally friendly freeze dryer for 24 h and H5P5 aerogels were obtained (−89 °C under vacuum). In this paper, H and P represent the mass percentages of HNTs and PVOH in the wet gel stage, respectively. The fabrication process of HNT/PVOH aerogels is depicted in Scheme 1.

2.3 Characterization

The density of HNTs/PVOH aerogel was calculated from the sample weight divided by its volume.

The morphology of the aerogel was observed using SEM (Hitachi S-4800), operated at an accelerating voltage of 10.0 kV, and a TEM (JEOL 1011) operated at an accelerating voltage of 100 kV.

The thermal conductivity test was performed by using a TC3000E system (TC3000E, XIA TECH, CHN), and the operating current range was 0–10 mA. The samples were both rectangular and five measurements were taken for each sample to take the average.

Compression test was carried out on an electronic universal testing machine (CMT 6104 SANS, GER). Five measurements were taken for each sample to take the average.

TGA (Pyris Diamond TG/DTA, Seiko Instruments Inc.) was conducted in nitrogen atmosphere from 25 to 500 °C at a heating rate of 5 °C min^{-1}.

3 Results and discussion

Figure 1 shows the pictures of wet gel and freeze-dried HNT/PVOH aerogels with different H:P mass ratios. With increasing HNT content in the samples, crack-free aerogels were obtained. These materials did not exhibit noticeable shrinkage during the freeze-drying process, probably due to the strong interactions between PVOH molecular chains [28]. Physical properties, including linear shrinkage, density, thermal conductivity, and compressive strength, are summarized in Table 1. With H:P ratio decreasing

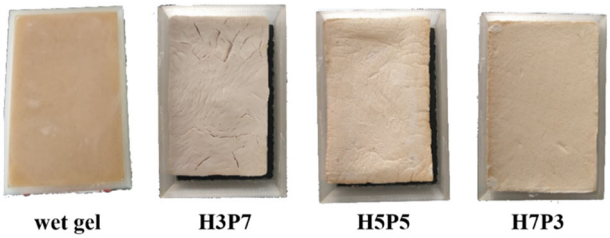

Fig. 1 Photographs of wet gel and freeze-dried halloysite nanotube/polyvinyl alcohol aerogels with different H:P mass ratios

Table 1 Physical properties of freeze-dried HNT/PVOH aerogels with different H:P mass ratios

Property	H0P10	H3P7	H5P5	H7P3
Linear shrinkage	~32%	~17%	~9%	~5%
Density (mg cm^{-3})	50 ± 1	75 ± 1	88 ± 1	104 ± 2
Thermal conductivity (W m^{-1} K^{-1})	0.034 ± 0.001	0.032 ± 0.001	0.030 ± 0.001	0.029 ± 0.001
Compressive strength (MPa)	0.4 ± 0.1	1.6 ± 0.1	2.3 ± 0.1	2.9 ± 0.1

HNT/PVOH halloysite nanotube/polyvinyl alcohol

gradually, the shrinkage percentage of HNT/PVOH aerogel composites increased remarkably, and the density decreased slightly. This could be ascribed to the presence of HNTs, which can effectively inhibit the contraction of composite aerogels during the freeze-drying process. Another possible reason was that the addition of HNTs allowed the composite to form a broad network, effectively reducing the volume shrinkage.

Wet gel samples with different H:P ratios exhibited shrinkage after drying, and the linear shrinkage rates of the four (H0P10, H3P7, H5P5, and H7P3) aerogels compared with the original wet gel were about 32, 17, 9, and 5%, respectively. Figure 2 is a schematic diagram of the shrinkage of HNTs/PVOH aerogel during the freeze-dried process. Wet gel samples were placed in an environment of −25 °C; water between the colloidal network was frozen to ice crystals and this process produced slight volume expansion [29]. The samples were then placed in an

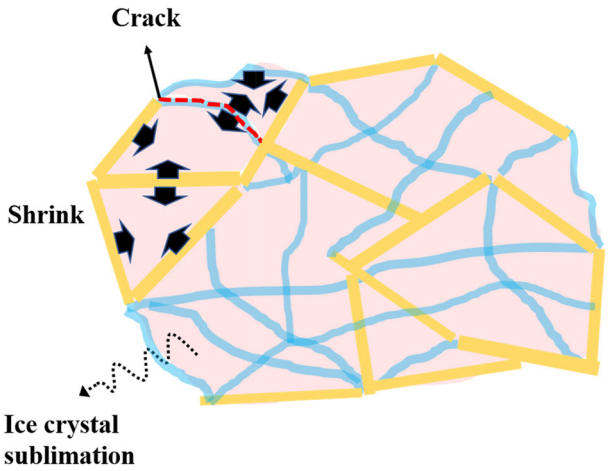

Fig. 2 Schematic diagram of the shrinkage of halloysite nanotube/polyvinyl alcohol aerogel during the freeze-drying process

environmentally friendly freeze dryer and the ice crystals began to sublime. The capillary force between the ice crystal and gel made the network shrink. The H0P10 sample had a low resistance to deformation due to the low strength of PVOH, and thus produced a large shrinkage and some cracks. Therefore, increasing the content of HNTs is a good solution to prevent shrinkage and cracking. We obtained a crack-free aerogel with a linear shrinkage of only 5% at H:P = 7:3.

Figure 3 shows the low- and high-magnification SEM images of HNT/PVOH aerogels with different mass ratios of HNT:PVOH. These SEM images confirm the above analysis of the linear shrinkage of HNT/PVOH aerogel composites. When HNTs were added, a harder and wider network was formed, which inhibited linear shrinkage. It is obvious that the morphology of the HNT/PVOH aerogels varies considerably with the changes of HNT:PVOH. The microstructure of pure PVOH material was composed of inhomogeneous PVOH lamellae and a small amount of PVOH network, as shown in Fig. 3a, b. For the sample of H3P7 in Fig. 3c, d, the PVOH molecular chains were intertwined with each other to form network structures existing between the interlayers, while the HNTs were attached to the PVOH framework. However, the microstructure of the H5P5 sample had changed obviously with the content of HNTs decreased and PVOH increased, and the overall morphology was a uniform three-dimensional porous structure (Fig. 3e). We can observe in Fig. 3f that the formation of a porous network structure was primarily due to the overlap of PVOH, and HNTs were fixed and connected with these organic materials to maintain a unique structure. As the HNT component was further increased, the aerogel maintained an overall uniform network structure (Fig. 3g), but formed a locally dense PVOH three-dimensional network (Fig. 3h).

Figure 4 shows TEM images of the H7P3 aerogel. As shown in Fig. 4a, the homogeneous three-dimensional network structure can be observed, HNTs were distributed uniformly, and pore size varied between tens and hundreds of nanometers in the sample. Furthermore, it was obvious to notice the typical nanotubular structure of HNTs and PVOH molecule chains on the HNT surface in Fig. 4b. This phenomenon suggested that PVOH molecules possessed good compatibility with HNTs, which was beneficial to enhance the dispersion and interfacial interaction of HNTs with PVOH molecular chains. The results were in good agreement with previous SEM information.

Compressive strength of different H:P ratios of HNT/PVOH aerogels are presented in Table 1. It shows that the addition of HNTs leads to a significant increase in the compressive strength of HNT/PVOH aerogels, and the strength of aerogels increases with the enhancement in the content of HNTs accordingly. This phenomenon can be illustrated by the models displayed in Fig. 5. Black arrows indicate the resistance of PVOH inside the aerogel while it is under stress, and red arrows are resistance generated by HNTs. It is clear that, with the HNT content increase, the number of red arrows will increase and black arrows decrease. Literature from both theoretical simulation and experimental verification shares a common viewpoint that the strength of HNTs is much higher than that of PVOH [8, 30, 31]. Also, red arrows are more resistant than black ones in this model. The compressive strength of the samples increases from 1.6 MPa of H3P7 to 2.9 MPa of H7P3.

The microstructure model of the HNT/PVOH aerogel (Fig. 6) can be plotted from SEM and TEM images. PVOH was adsorbed and bound to the outer portions of HNTs, and natural untreated tubular clay built a stereonetwork structure by means of PVOH. Depending on the ratio of HNT:PVOH, unattached PVOH would cross-link each other to form a three-dimensional structure with a smaller pore size between the HNT and PVOH aerogel. With such a good porous structure, the aerogel had excellent performance such as lightweight, good mechanical properties, and good heat insulation.

As shown in Fig. 6, effective thermal conductivity λ_e of HNT/PVOH aerogel is mainly composed of three parts: contribution of radiation heat conduction λ_r, contribution of solid heat conduction λ_s, and gaseous heat conduction λ_g [32, 33]. λ_e could be expressed as Eq. (1):

$$\lambda_e = \lambda_r + \lambda_s + \lambda_g \quad (1)$$

The thermal conductivities of various H/P aerogels are listed in Table 1. For raw materials, as PVOH has lower thermal conductivity than HNTs, the overall insulation performance of H/P aerogels may become worse with the increase of H:P ratios. However, the results indicated that, with the increase of HNT content, the thermal conductivity

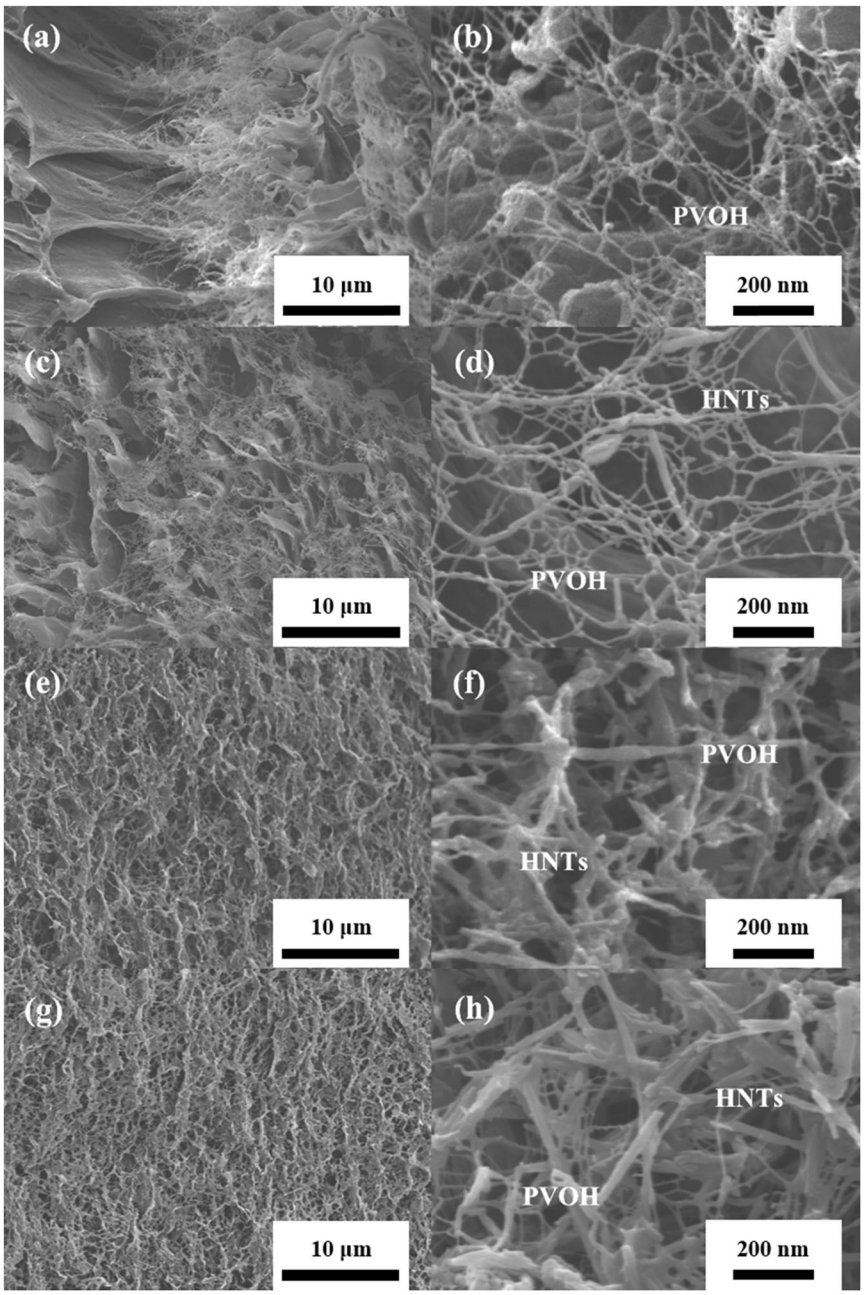

Fig. 3 Low- and high-magnification scanning electron microscopic images of halloysite nanotube/polyvinyl alcohol (PVOH) aerogels with different H:P mass ratios: (**a**, **b**) neat PVOH; (**c**, **d**) H3P7; (**e**, **f**) H5P5; (**g**, **h**) H7P3

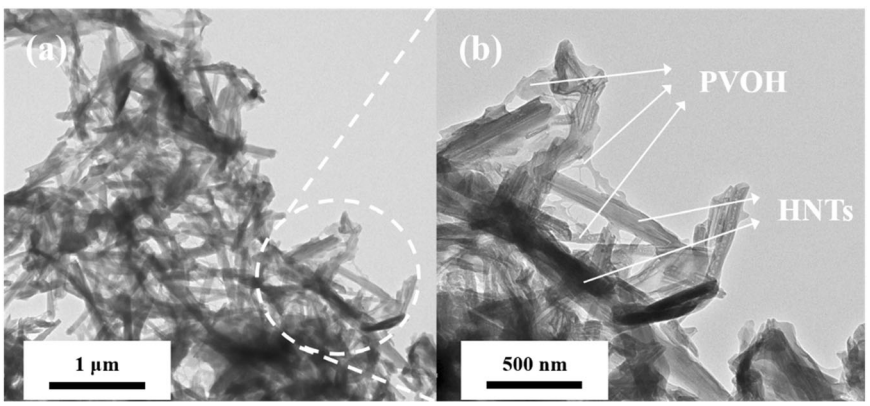

Fig. 4 Low- and high-magnification transmission electron microscopic images of the H7P3 aerogel

decreases gradually, and this could be attributed to three factors. The first one is the presence of HNT–PVOH interface heat transfer resistance [34–36]. When the heat flow passed through the PVOH–HNT interface, the interface heat transfer resistance increased the obstruction of phonon heat transfer at the interface, and then the thermal conductivity decreased (interface thermal resistance in Fig. 6). As the ratio of H:P increased, there would be more PVOH adhered to HNTs, then HNT–PVOH interfaces increased, and λ_s would decrease. If the content of PVOH were too low to produce PVOH–HNT interfaces, the thermal insulation began to become worse. The second one was because of the increase in the mean-free path of gas molecules [37, 38]. From high-magnification SEM images, the addition of HNTs would form a relatively dense network locally in the sample. Owing to the phonon filtration in the small interface contact area, the longer the mean-free path of gaseous heat transfer, the lower the equivalent heat conduction λ_g became. The third one was due to the barrier effect of HNTs [39, 40]. The uniform distribution of HNTs in the aerogel formed a number of barriers that could effectively absorb and reflect thermal radiation, which caused a decrease in λ_r. However, in this study, the materials we studied were usually used in room-temperature environments, such as buildings, where radiant heat conduction accounted for only a very small fraction of the effective thermal conductivity. Based on the above three factors, the thermal conductivity would decrease with the H:P ratio increase, but from the influencing factors and the trend of experimental data, it was predicted that λ_e would decrease to a minimum and then increase.

Thermal stabilities of HNT/PVOH aerogels with different H:P mass ratios were investigated by heat treatments under N_2 atmosphere from 25 to 500 °C, and the corresponding thermogravimetric curves are given in Fig. 7. The TGA curves of all samples reveal three main stages of mass loss, which are consistent with previous literatures and reports [27, 41]. The three main mass loss stages of H0P10 aerogel are 50–220 °C, 250–350 °C, and 370–470 °C, respectively. The first stage corresponded to the loss of bound water, the second one mainly contained volatility of organic compounds and formation of conjugated unsaturated polyenes, and the third stage showed that polyene residues are degraded by intramolecular cyclization to olefins and alkanes, as well as aromatic hydrocarbons [42, 43]. There are only slight differences between H0P10 and the other three HNT/PVOH aerogels at the first mass loss stage, where the mass loss of samples that have HNTs also includes the loss of bound water to HNTs. At the second stage, there is almost no mass loss of HNTs [44], so the four samples show a huge difference: the higher HNT percentage the samples have, the less the mass loss. After the mass loss in the second stage, the PVOH residual content is very small, so the difference between the four samples in the third stage is also very small, mainly of the degradation of polyene residues.

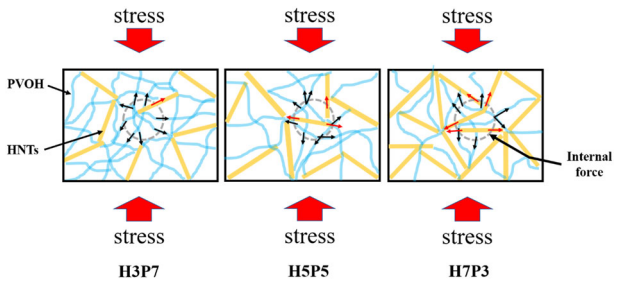

Fig. 5 Compressive strength models with different H:P ratio aerogels

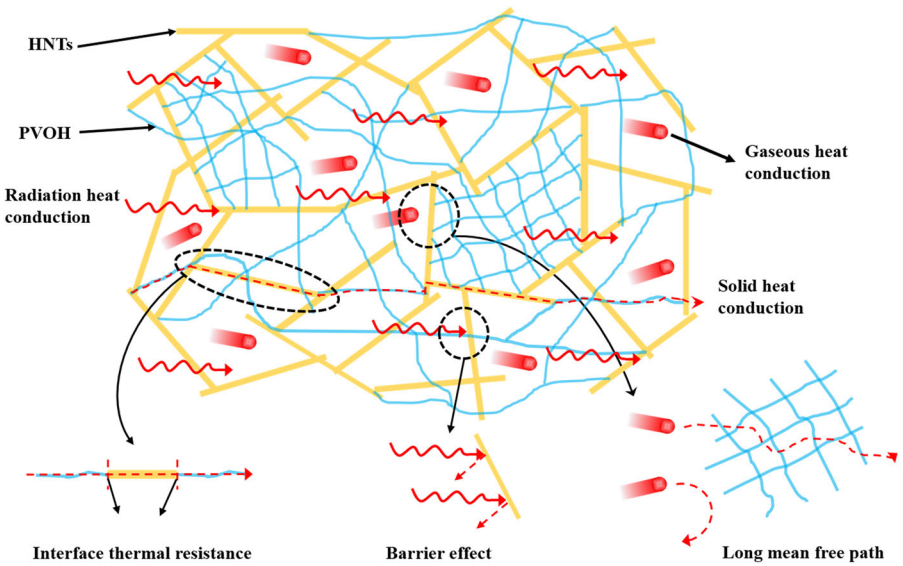

Fig. 6 Heat transfer model of halloysite nanotube/polyvinyl alcohol aerogel

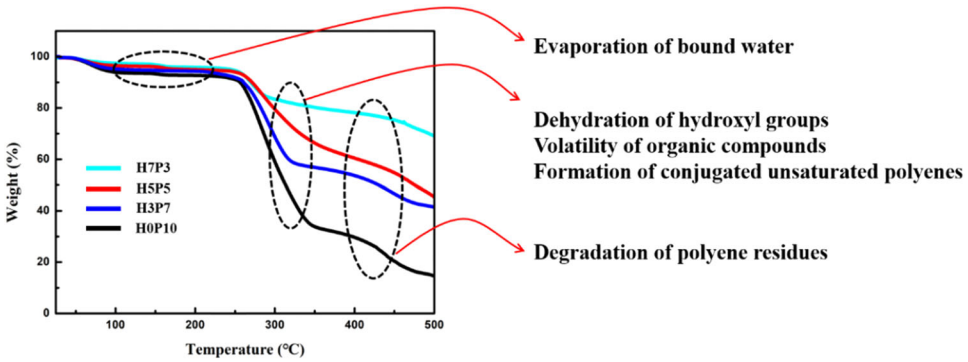

Fig. 7 Thermogravimetric analysis curves of aerogels with different H:P ratios under constant heating rate

Table 2 Residual percentages of different H:P ratios of HNT/PVOH aerogels, HNTs, and PVOH calculated by Eqs. (2) and (3)

	H7P3		H5P5		H3P7		H0P10	
Heat treatment	Before	After	Before	After	Before	After	Before	After
HNTs (%)	70	67.3	50	38.1	30	31.2	0	0
PVOH (%)	30	4.4	50	7.3	70	10.2	100	14.6
H/P aerogel (%)	100	71.7 ± 0.1	100	45.4 ± 0.1	100	41.4 ± 0.1	100	14.6 ± 0.1

HNT/PVOH halloysite nanotube/polyvinyl alcohol

After heat treatment, the residual percentages of the samples from H0P10, H3P7, H5P5, and H7P3 are 71.7, 45.4, 41.4, and 14.6%, respectively. Since the H0P10 sample does not contain HNTs, we can conclude that the residual amount of PVOH after heat treatment at 500 °C is 14.6% (the amount of cross-linking agent is small and can be ignored). The residual percentage of HNTs (R_H) and PVOH (R_P) in different H:P ratio aerogels can be calculated by Eqs. (2) and (3)

$$R_P = S_{H/P} \times 14.6\% \quad (2)$$

$$R_H = R_{H/P} - R_P \quad (3)$$

where $S_{H/P}$ represents the mass percentage of PVOH in the aerogel samples before heat treatment, and $R_{H/P}$ represents the residual percentage of H/P aerogels after heat treatment. The calculated residual percentages of HNTs and PVOH are listed in Table 2 according to Eqs. (2) and (3). As shown in Table 2, the content of HNTs in H3P7 aerogel is 30% and 31.2% before and after heat treatment, respectively, which is obviously unreasonable. The result indicated that the addition of HNTs improved the thermal stability of PVOH at 500 °C, resulting in the actual residual ratio of >14.6% for PVOH.

Figure 8 exhibits the TEM image of H7P3 aerogel after thermal treatment. We could observe that, after the heat treatment of 500 °C, there are few left PVOH adhered to HNTs, and the mass loss of aerogels was mainly due to the degradation of PVOH. However, as a support for the three-dimensional structure, the large loss of PVOH did not result in catastrophic damage to the HNT/PVOH aerogel. This was due to the fact that residues of PVOH degradation remained on HNTs, so that the three-dimensional network structure could be well preserved. This clay aerogel material that could maintain a three-dimensional structure at 500 °C would be of great help in many fields.

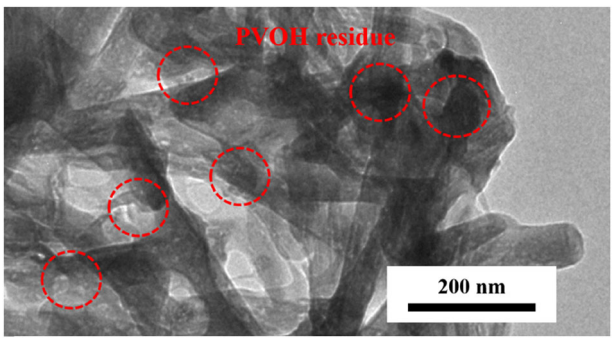

Fig. 8 Transmission electron microscopic image of H7P3 aerogel after treatment at 500 °C

4 Conclusions

A facile, efficient, and environmentally friendly strategy was utilized to fabricate HNT/PVOH aerogel composites. In these aerogels, PVOH was adhered to HNTs to form a polymer-assisted three-dimensional network. With the HNT content increased, the linear shrinkage was reduced from 17% of H3P7 to 5% of H7P3. SEM and TEM images indicated that HNTs were uniformly distributed throughout the aerogels, and the addition of HNTs caused the PVOH to

form a locally dense three-dimensional network. The thermal conductivity of clay aerogels was varied between 0.034 and 0.029 $W m^{-1} K^{-1}$, and it decreased moderately as the HNT content increased. With the value of H:P increased, the compressive strength and thermal stability effectively improved, and the complete network structure could be maintained after heat treatment at 500 °C. At H:P = 7:3, the obtained H7P3 aerogel had a compressive strength of 2.9 MPa and a thermal conductivity of 0.029 $W m^{-1} K^{-1}$. This kind of aerogel with facile preparation process and such properties could be promising for applications in building insulation, aerospace, chemical production, etc.

Acknowledgements This work was financially supported by the National Natural Science Foundation of China (Nos. 51772202 and 51472175).

Compliance with ethical standards

Conflict of interest The authors declare that they have no conflict of interest.

References

1. Chen HB, Chiou BS, Wang YZ, Schiraldi DA (2013) Biodegradable pectin/clay aerogels. ACS Appl Mater Interfaces 5 (5):1715–1721
2. Bandi S, Bell M, Schiraldi DA (2005) Temperature-responsive clay aerogel-polymer composites. Macromolecules 38 (22):9216–9220
3. Finlay K, Gawryla MD, Schiraldi DA (2008) Biologically based fiber-reinforced/clay aerogel composites. Ind Eng Chem Res 47 (3):615–619
4. Wang L, Sánchez-Soto M, Maspoch ML (2013) Polymer/clay aerogel composites with flame retardant agents: mechanical, thermal and fire behavior. Mater Design 52(2013):609–614
5. Liu A, Medina L, Berglund LA (2017) High-strength nanocomposite aerogels of ternary composition: poly(vinyl alcohol), clay, and cellulose nanofibrils. ACS Appl Mater Interfaces 9 (7):6453–6461
6. Wang L, Sánchez-Soto M, Abt T, Maspoch ML, Santana OO (2016) Microwave-crosslinked bio-based starch/clay aerogels. Polym Int 65(8):899–904
7. Lu Y, Wu H, Chen Q (2015) Facile preparation of fracture-free pectin/clay aerogel monoliths. Mater Res Innov 19(sup2):s2-s46–s2-51
8. Lvov Y, Wang WC, Zhang LQ, Fakhrullin R (2016) Halloysite clay nanotubes for loading and sustained release of functional compounds. Adv Mater 28(6):1227–1250
9. Gaaz T, Kadhum A, Michael P, Al-Amiery A, Sulong A, Nassir M, Jaaz A (2017) Unique halloysite nanotubes-polyvinyl alcohol-polyvinylpyrrolidone composite complemented with physicochemical characterization. Polymer 9(12):207
10. Cheng ZL, Qin XX, Liu Z, Qin DZ (2016) Electrospinning preparation and mechanical properties of PVA/HNTs composite nanofibers. Polym Adv Technol 28(6):768–774
11. Liu MX, Jia ZX, Jia DM, Zhou CR (2014) Recent advance in research on halloysite nanotubes-polymer nanocomposite. Prog Polym Sci 39(8):1498–1525
12. Lvov YM, Shchukin DG, Möhwald H, Price RR (2008) Halloysite clay nanotubes for controlled release of protective agents. ACS Nano 2(5):814–820
13. Kang HJ, Liu XR, Zhang SF, Li JZ (2017) Functionalization of halloysite nanotubes (HNTs) via mussel-inspired surface modification and silane grafting for HNTs/soy protein isolate nanocomposite film preparation. RSC Adv 7(39):24140–24148
14. Cunha DA, Rodrigues NS, Souza LC, Lomonaco D, Rodrigues FP, Degrazia FW, Collares FM, Sauro S, Saboia VPA (2018) Physicochemical and microbiological assessment of an experimental composite doped with triclosan-loaded halloysite nanotubes. Materials 11(7):1080
15. De Silva RT, Pasbakhsh P, Goh KL, Chai SP, Ismail H (2013) Physico-chemical characterisation of chitosan/halloysite composite membranes. Polym Test 32(2):265–271
16. Khunová V, Kelnar I, Kristóf J, Dybal J, Kratochvíl J, Kaprálková L (2015) The effect of urea and urea-modified halloysite on performance of PCL. J Therm Anal Calorim 120(2):1283–1291
17. Yang YX, Hai SK, Zhang WN (2017) Research on performance of PHA composites reinforced by HNTs. Plastics Sci Technol 46 (1):76–79
18. Liu HL, Wei N, He X, An GQ, Xuan YJ (2018) Facile fabrication and characterization of novel three-dimensional halloysite nanotubes/graphene oxide composite aerogels for waste water treatment. Ferroelectrics 528(1):22–30
19. Zhang Y, Jing OY, Yang HM (2014) Metal oxide nanoparticles deposited onto carbon-coated halloysite nanotubes. Appl Clay Sci 95:252–259
20. Errais E, Duplay J, Darragi F, M'Rabet I, Aubert A, Huber F, Morvan G (2011) Efficient anionic dye adsorption on natural untreated clay: kinetic study and thermodynamic parameters. Desalination 275(1–3):74–81
21. Hao A, Wong I, Wu H, Lisco B, Ong B, Sallean A, Butler S, Londa M, Koo JH (2014) Mechanical, thermal, and flame-retardant performance of polyamide 11-halloysite nanotube nanocomposites. J Mater Sci 50(1):157–167
22. Jamaludin NA, Inuwa IM, Hassan A, Othman N, Jawaid M (2015) Mechanical and thermal properties of SEBS-g-MA compatibilized halloysite nanotubes reinforced polyethylene terephthalate/polycarbonate/nanocomposites. J Appl Polym Sci 132(39):42608
23. Erdogan AR, Kaygusuz L, Kaynak C (2013) Influences of aminosilanization of halloysite nanotubes on the mechanical properties of polyamide-6 nanocomposites. Polym Composite 35 (7):1350–1361
24. Liu HL, He X, Li HY, Yang AW, Xiao R, Wei N (2017) Preparation and properties of HNTs/SiO_2 composite aerogels. J Synth Cryst 46(11):2277–2282
25. Mraz J, Jheeta P, Gescher A, Hyland R, Thummel K, Threadgill MD (1993) Investigation of the mechanistic basis of N,N-dimethylformamide toxicity. Metabolism of N,N-dimethylformamide and its deuterated isotopomers by cytochrome P450 2E1. Chem Res Toxicol 6(2):197–207
26. Lee M, Choi Y, Matsugi K, Sasaki G, Kelimu T (2013) Effect of SiO_2 amount on microstructures and tensile properties of alumina short fiber-reinforced composites by low-pressure infiltration method. J Compos Mater 48(27):3435–3441
27. Chen HB, Liu B, Huang W, Wang JS, Zeng G, Wu WH (2014) Fabrication and properties of irradiation-cross-linked polyvinyl alcohol/clay aerogel composites. ACS Appl Mater Interfaces 6 (18):16227–16236
28. Chen HB, Hollinger E, Wang YZ, Schiraldi DA (2014) Facile fabrication of polyvinyl alcohol gels and derivative aerogels. Polymer 55(1):380–384

29. Anderson AM, Worster MG (2012) Periodic ice banding in freezing colloidal dispersions. Langmuir 28(48):16512–16523
30. Zhou T, Cheng XD, Pan YL, Li CC, Gong LL (2018) Mechanical performance and thermal stability of polyvinyl alcohol–cellulose aerogels by freeze drying. Cellulose 26(3):1747–1755
31. Cheng ZH, DeGracia K, Schiraldi DA (2018) Sustainable, low flammability, mechanically-strong poly(vinyl alcohol) aerogels. Polymers 10(10):1102
32. He C, He YL, Xie T, Liu Q (2013) Predictions of the effective thermal conductivity for aerogel-fiber composite insulation materials using lattice Boltzmann method. J Eng Thermophys 34:742–745
33. Qu ZG, Fu YD, Liu Y, Zhou L (2018) Approach for predicting effective thermal conductivity of aerogel materials through a modified lattice Boltzmann method. Appl Therm Eng 132:730–739
34. Xue T, Zhang X, Tamma KK (2018) A two-field state-based peridynamic theory for thermal contact problems. J Comput Phys. https://doi.org/10.1016/j.jcp.2018.08.014
35. Vishweshwara PS, Gnanasekaran N, Arun M (2018) Inverse estimation of interfacial heat transfer coefficient during the solidification of Sn-5wt%Pb alloy using evolutionary algorithm. Adv Mater Metallurgy. https://doi.org/10.1007/978-981-13-1780-4_23
36. Pang XM, Zhou JQ, Yang JX, Liao MH (2016) Effective thermal conductivity of composite materials containing pore and interface thermal resistance. Chin J Nonferrous 26(8):1668–1674
37. Li ZY, Zhu CY, Zhao XP (2017) A theoretical and numerical study on the gas-contributed thermal conductivity in aerogel. Int J Heat Mass Trans 108:1982–1990
38. Wei GS, Wang LX, Chen L, Du XZ, Xu C, Zhang XX (2015) Analysis of gas molecule mean free path and gaseous thermal conductivity in confined nanoporous structures. Int J Thermophys 36(10–11):2953–2966
39. Zhang C, Kan AK, Meng C, Guo ZP, Cao D, Xu Z (2016) Research status of insulative aerogel composite material. Chin Refrig Technol 36(4):61–67
40. Du ML, Guo BC, Jia DM (2006) Thermal stability and flame retardant effects of halloysite nanotubes on poly(propylene). Eur Polym J 42(6):1362–1369
41. Alhassan SM, Qutubuddin S, Schiraldi DA (2015) Mechanically strong ice-templated laponite/polyvinyl alcohol aerogels. Mater Lett 157:155–157
42. Rowe AA, Tajvidi M, Gardner DJ (2016) Thermal stability of cellulose nanomaterials and their composites with polyvinyl alcohol (PVA). J Therm Anal Calorim 126(3):1371–1386
43. Liu YX, Fan LL, Mo XZ, Pang JY, Yang F (2017) Thermal decomposition behavior of TPS/PVA blends. China Synth Resin Plastics 34(6):43–52
44. Paran SMR, Vahabi H, Jouyandeh M, Ducos F, Formela K, Saeb MR (2019) Thermal decomposition kinetics of dynamically vulcanized polyamide 6-acrylonitrile butadiene rubber-halloysite nanotube nanocomposites. J Appl Polym Sci 136(20):47483